Weak-field asymptotic theory of tunneling ionization of the hydrogen molecule including core polarization, spectator nucleus, and internuclear motion effects

Hirokazu Matsui,[1] Oleg I. Tolstikhin,[2] and Toru Morishita[3,1]

[1]*Department of Engineering Science, The University of Electro-Communications, 1-5-1 Chofu-ga-oka, Chofu-shi, Tokyo 182-8585, Japan*

[2]*Moscow Institute of Physics and Technology, Dolgoprudny 141700, Russia*

[3]*Institute for Advanced Science, The University of Electro-Communications, 1-5-1 Chofu-ga-oka, Chofu-shi, Tokyo 182-8585, Japan*

(Received 5 June 2020; accepted 16 February 2021; published 1 March 2021)

We present a state-of-the-art theory of tunneling ionization of the hydrogen molecule in a static electric field. The theory is based on the leading-order many-electron weak-field asymptotic theory and successively incorporates core polarization, spectator nucleus, and internuclear motion effects. The predictions of the theory are compared with *ab initio* calculations of the ionization rate of H_2 with frozen nuclei and experimental results on the anisotropy of strong-field ionization of H_2 and D_2. The comparison reveals the relative role of the different effects. We show that all the effects should be taken into account in order to achieve good agreement with the *ab initio* and experimental results.

DOI: 10.1103/PhysRevA.103.033102

I. INTRODUCTION

The ionization of atoms and molecules in a strong laser field is the first fundamental step for all phenomena observed and studied in strong-field physics [1]. Typical laser pulses used in strong-field experiments satisfy two conditions. First, they have sufficiently high intensity ($I \sim 10^{14}$ W/cm^2) and low frequency ($\lambda \gtrsim 800$ nm), so that the ionization proceeds in the adiabatic regime [2], as if the laser field were static. Second, the laser field is rather weak compared to characteristic atomic fields, so that the release of an electron occurs in the tunneling (under-the-barrier) regime. The weak-field asymptotic theory (WFAT) of tunneling ionization in a static electric field [3] suggests a general theoretical platform for studying the ionization step in strong-field processes under these conditions.

The WFAT is based on the asymptotic expansion of the ionization rate in the strength F of the ionizing field. By construction, this theory becomes exact at $F \to 0$ and its error grows as F grows. The original one-electron leading-order theory [3] was extended to the first-order correction terms in the asymptotic expansion of the ionization rate [4] and generalized to many-electron systems (ME-WFAT) in the leading-order approximation [5] and including the first-order terms [6,7]. The theory was validated by comparison with accurate *ab initio* calculations. The good quantitative performance of the one-electron WFAT was confirmed by calculations for noble gas atoms treated in the single-active-electron approximation [4] and the hydrogen molecular ion H_2^+ [8]. Converged fully correlated *ab initio* calculations of ionization rates for systems with more than one electron are available only for H^- [9], He [10–12], Li [13], and the hydrogen molecule H_2 [14,15]; note that great progress in extending such calculations to larger systems is taking place [15,16]. In Ref. [6], an analytical formula for the ionization rate of two-electron atoms obtained within the ME-WFAT including the first-order terms was presented. This formula reproduces the *ab initio* results for He [10–12] with an error less than 25% up to $F = 0.2$ a.u. One obvious advantage of having such a reliable analytical theory stems from its usefulness for applications, especially in situations where *ab initio* calculations are not feasible. We mention that the WFAT has been implemented for diatomic [17,18], triatomic [17,19], and arbitrary polyatomic [20,21] molecules treated in the Hartree-Fock approximation (WFAT-HF) and successfully applied to the analysis of experiments [22–25]. But there also exists another advantage: the theory provides physical insight into the tunneling ionization process enabling one to investigate how the different properties of the system affect the ionization rate. This was demonstrated by the application of the ME-WFAT to two-electron atoms [6,7]. In this paper, we present a similar analysis for the hydrogen molecule.

There are several effects not accounted for by the original formulation of the ME-WFAT [5] which are relevant to H_2 and should be included in the analysis. First, the ground $1s\sigma$ state of the molecular ion H_2^+ is nearly degenerate with the first excited $2p\sigma$ state at large internuclear distances. This results in large polarizability of the core in the ionization of H_2, which affects the ionization rate. Second, it has been shown recently [26] that for molecules with large internuclear distances the WFAT rate formula must be modified to account for the effect of spectator nuclei on the ionization rate from a parent nucleus. Third, the internuclear motion should be included into consideration. The isotope effect in tunneling ionization of hydrogen molecules predicted theoretically [27] and observed experimentally [28] demonstrates the importance of its effect on the ionization rate. We incorporate all these effects on the basis of the leading-order ME-WFAT [5], which results in a state-of-the-art theory of tunneling ionization of H_2.

To gauge the theory, we compare its results with *ab initio* calculations of the ionization rate of H_2 with frozen nuclei [14,15]. Then we apply it to the analysis of benchmark

experiments where an anisotropy in tunneling ionization of H_2 [29] and D_2 [30] was measured. The orientation dependence of the ionization rate of H_2 was studied by different theoretical methods, including molecular Ammosov-Delone-Krainov model [31,32], WFAT-HF [17,18,27], ME-WFAT [5,33], time-dependent Schrödinger equation [30,34–37], time-dependent density functional theory [38,39], strong-field approximation [29,40], and semiclassical models [41], and has recently attracted new interest experimentally [42]; see also a review article [43]. However, as far as we know, the results of Refs. [29,30] have not been reproduced satisfactorily. In particular, the isotope effect on the anisotropy of the ionization rate was not described. The main goal of this paper, which has actually motivated the whole study, is to contribute to resolving this issue.

The paper is organized as follows. In Sec. II, we formulate the present theory. In Sec. III, we discuss its numerical implementation. In Sec. IV, the predictions of the theory are compared with *ab initio* calculations [14,15] and experiments [29,30]. Section V concludes the paper.

II. THEORY

In this section, we present the theory used in the calculations reported in subsequent sections. We first summarize the leading-order ME-WFAT, which provides the basis for all further extensions, and then successively incorporate three effects mentioned in the title.

A. Many-electron weak-field asymptotic theory

We begin with summarizing basic equations of the ME-WFAT [5] for the hydrogen molecule with frozen nuclei. The ionizing electric field is directed along the z axis, $\mathbf{F} = (0, 0, F)$. The nuclei are located in the (x, z) plane symmetrically with respect to the origin. Let $\mathbf{R} = (R\sin\beta, 0, R\cos\beta)$, where R is the internuclear distance and β is the angle between the internuclear axis and the field. We assume that the molecule H_2 is initially in the ground two-electron state $^1\Sigma_g^+$ defined by (atomic units are used throughout the paper)

$$\left[-\frac{\Delta_1}{2} - \frac{\Delta_2}{2} + V(\mathbf{r}_1) + V(\mathbf{r}_2) + \frac{1}{|\mathbf{r}_1 - \mathbf{r}_2|} - E_0^{(2)}(R)\right] \times \psi_0^{(2)}(\mathbf{r}_1, \mathbf{r}_2; \mathbf{R}) = 0, \tag{1}$$

where

$$V(\mathbf{r}) = -\frac{1}{|\mathbf{r} + \mathbf{R}/2|} - \frac{1}{|\mathbf{r} - \mathbf{R}/2|}. \tag{2}$$

The final one-electron states of the molecular ion H_2^+ are defined by

$$\left[-\frac{\Delta}{2} + V(\mathbf{r}) - E_n^{(1)}(R)\right]\psi_n^{(1)}(\mathbf{r}; \mathbf{R}) = 0, \tag{3}$$

where $n = 1s\sigma, 2p\sigma, \ldots$ denotes a set of united-atom quantum numbers. The energies and wave functions of all these states depend on R as a parameter. The wave functions additionally depend on β included in the argument $\mathbf{R}$. Being motivated by the comparison with experiments [29,30], in the calculations we consider only parallel and perpendicular orientations of the molecule with respect to the field corresponding to $\beta = 0^\circ$ and 90°, respectively; we will use the notation $\mathbf{R}_\parallel = (0, 0, R)$ and $\mathbf{R}_\perp = (R, 0, 0)$. However, in formulating the theory it is convenient to treat arbitrary β. All the wave functions introduced above are assumed to be real and normalized to unity.

In the weak-field limit, $F \to 0$, the ionization process in which the molecular ion is left in a given state n is described by the Dyson orbital

$$\upsilon_n(\mathbf{r}; \mathbf{R}) = \sqrt{2}\int \psi_n^{(1)}(\mathbf{r}_1; \mathbf{R})\psi_0^{(2)}(\mathbf{r}_1, \mathbf{r}; \mathbf{R})\, d\mathbf{r}_1. \tag{4}$$

This orbital is considered as a function of parabolic coordinates

$$\xi = r + z, \quad 0 \leqslant \xi < \infty, \tag{5a}$$

$$\eta = r - z, \quad 0 \leqslant \eta < \infty, \tag{5b}$$

$$\varphi = \arctan(y/x), \quad 0 \leqslant \varphi < 2\pi. \tag{5c}$$

Tunneled electrons are driven by the field towards $z \to -\infty$, which corresponds to $\eta \to \infty$. The outgoing flux of electrons in this asymptotic region can be decomposed into ionization channels enumerated by n and parabolic quantum numbers $n_\xi = 0, 1, \ldots$ and $m = 0, \pm 1, \ldots$. For a given n, the dominant contribution to the flux comes from the channel with $n_\xi = m = 0$. The corresponding partial ionization rate is given by [5]

$$\Gamma_n^{(0)}(\mathbf{R}, F) = G_n^2(\mathbf{R})W(F, \varkappa_n(R)). \tag{6}$$

Here $G_n(\mathbf{R})$ is the structure factor,

$$G_n(\mathbf{R}) = \lim_{\eta\to\infty} G_n(\eta; \mathbf{R}), \tag{7}$$

where $G_n(\eta; \mathbf{R})$ is the structure function defined by

$$G_n(\eta; \mathbf{R}) = \sqrt{\frac{\varkappa}{2\pi}}\,\eta^{1-1/\varkappa}e^{\varkappa\eta/2} \times \int_0^\infty \int_0^{2\pi} e^{-\varkappa\xi/2}\upsilon_n(\mathbf{r}; \mathbf{R})\, d\xi\, d\varphi\Big|_{\varkappa=\varkappa_n(R)}, \tag{8}$$

$W(F, \varkappa)$ is the field factor,

$$W(F, \varkappa) = \frac{\varkappa}{2}\left(\frac{4\varkappa^2}{F}\right)^{2Z/\varkappa-1}\exp\left(-\frac{2\varkappa^3}{3F}\right), \tag{9}$$

where $Z = 1$ is the total charge of the molecular ion, and

$$\varkappa_n(R) = \sqrt{2I_n(R)}, \quad I_n(R) = E_n^{(1)}(R) - E_0^{(2)}(R), \tag{10}$$

where $I_n(R)$ is the field-free ionization potential. In Eq. (8), we have taken into account that both the initial and final states have zero dipole moments. Equation (6) gives the leading-order term in the asymptotic expansion of the partial ionization rate in F. The rates of tunneling ionization into excited states of the molecular ion are suppressed compared to that into the ground state $n = 1s\sigma$, because of the exponential factor in Eq. (9). Thus, the total ionization rate of the molecule in the leading-order approximation of the ME-WFAT is given by $\Gamma_{1s\sigma}^{(0)}(\mathbf{R}, F)$; we will refer to this approximation as ME-WFAT(0). It holds under the condition [3,4]

$$F \ll F_c(R) \approx \frac{\varkappa_{1s\sigma}^4(R)}{8|2Z - \varkappa_{1s\sigma}(R)|}, \tag{11}$$

where $F_c(R)$ is a critical field giving a boundary between tunneling and over-the-barrier ionization regimes. Note that the effects discussed below are treated as corrections on the basis of the ME-WFAT(0), so their inclusion does not modify the condition of applicability (11) of the theory.

B. Stark-shift and core polarization effects

The ME-WFAT was extended to the first-order correction terms in the asymptotic expansion of the ionization rate in F [6,7]. Physically, the corrections account for the second-order Stark shift and first-order distortion of the initial and final states caused by the ionizing field as well as for contributions from next-to-the-dominant ionization channels with $n_\xi = 0$ and $m = \pm 1$ [4,6,7]. So far, the first-order theory denoted by ME-WFAT(1) has been implemented as prescribed, without any additional approximations, only for two-electron atoms [6,7]. It would be very instructive to extend its implementation to two-electron diatomic molecules; this, however, is a rather difficult technical task. In this paper, we account for only a part of the first-order effects. Namely, we include the Stark shift for both the initial and final states. This is needed because the shift modifies the ionization potential, which strongly affects the ionization rate. As for distortion, we include it for the final state but neglect for the initial state. Such an approach is justified by the fact that the ground electronic state $^1\Sigma_g^+$ of H_2 for all internuclear distances R is well separated in energy from the other states, while the ground electronic state $1s\sigma$ of H_2^+ at large R is nearly degenerate with the lowest excited state $2p\sigma$. The degeneracy results in large polarizability of the core in tunneling ionization of H_2 at large R, which affects the ionization rate. Here, we take this core polarization effect into account.

The second-order Stark shift of the energy of the initial state is described by

$$E_0^{(2)}(\mathbf{R}, F) = E_0^{(2)}(R) - \tfrac{1}{2}\alpha(\mathbf{R})F^2, \tag{12}$$

where $\alpha(\mathbf{R})$ is the static polarizability of H_2. The Stark shift and distortion of the final state is described using an approach proposed in Ref. [26]. As one electron of H_2 tunnels, the other electron remaining in the molecular ion still interacts with the field, which causes polarization of the core. Following Ref. [26], this effect can be accounted for by replacing field-free one-electron states in the equations of ME-WFAT(0) by the corresponding Stark-mixed states defined by Eq. (3) with an additional term Fz in the Hamiltonian. The Stark-mixed states can be expanded in field-free states,

$$\psi_\alpha^{(1)}(\mathbf{r}; \mathbf{R}, F) = \sum_n c_n^\alpha(\mathbf{R}, F)\psi_n^{(1)}(\mathbf{r}; \mathbf{R}). \tag{13}$$

The coefficients $c_n^\alpha(\mathbf{R}, F)$ in the expansion and the energy of the state $E_\alpha^{(1)}(\mathbf{R}, F)$ can be found by solving the eigenvalue problem

$$\sum_m \left\{\left[E_n^{(1)}(R) - E_\alpha^{(1)}(\mathbf{R}, F)\right]\delta_{nm} + F z_{nm}(\mathbf{R})\right\} c_m^\alpha(\mathbf{R}, F) = 0, \tag{14}$$

where

$$z_{nm}(\mathbf{R}) = \int \psi_n^{(1)}(\mathbf{r}; \mathbf{R}) z \psi_m^{(1)}(\mathbf{r}; \mathbf{R})\, d\mathbf{r}. \tag{15}$$

We label these states by $\alpha = 1s\sigma, 2p\sigma, \ldots$ which indicates the field-free state from which they originate as the field is turned on. The ionization process in which the molecular ion is left in a given Stark-mixed state α is described by the Stark-mixed Dyson orbital defined similarly to Eq. (4),

$$\upsilon_\alpha(\mathbf{r}; \mathbf{R}, F) = \sqrt{2}\int \psi_\alpha^{(1)}(\mathbf{r}_1; \mathbf{R}, F)\psi_0^{(2)}(\mathbf{r}_1, \mathbf{r}; \mathbf{R})\, d\mathbf{r}_1. \tag{16}$$

The corresponding partial ionization rate is given by [26]

$$\Gamma_\alpha^{\mathrm{P}}(\mathbf{R}, F) = G_\alpha^2(\mathbf{R}, F) W(F, \varkappa_\alpha(\mathbf{R}, F)), \tag{17}$$

where

$$G_\alpha(\mathbf{R}, F) = \sum_n c_n^\alpha(\mathbf{R}, F) G_n(\mathbf{R}) \tag{18}$$

and

$$\varkappa_\alpha(\mathbf{R}, F) = \sqrt{2I_\alpha(\mathbf{R}, F)},$$
$$I_\alpha(\mathbf{R}, F) = E_\alpha^{(1)}(\mathbf{R}, F) - E_0^{(2)}(\mathbf{R}, F). \tag{19}$$

Here $I_\alpha(\mathbf{R}, F)$ is the Stark-shifted ionization potential. The dominant contribution to the total ionization rate of the molecule comes from ionization into the lowest Stark-mixed state $\alpha = 1s\sigma$. The rate is thus given by $\Gamma_{1s\sigma}^{\mathrm{P}}(\mathbf{R}, F)$; we will refer to this approximation as ME-WFAT-P, where P stands for polarization. Note that the leading-order term in the asymptotic expansion of $\Gamma_{1s\sigma}^{\mathrm{P}}(\mathbf{R}, F)$ in F coincides with $\Gamma_{1s\sigma}^{(0)}(\mathbf{R}, F)$, the difference between the two approximations arises from higher-order terms which account for the Stark shift of the initial and final states and polarization of the core. Let us repeat that in contrast to ME-WFAT(1) [6,7], which is based on the consistent asymptotic expansion in F, ME-WFAT-P only partially accounts for the first-order correction terms, but at the same time includes some of the higher-order terms.

C. Spectator nucleus effect

The field factor (9) describes tunneling of an electron through the barrier separating the potential well created by the molecular ion from the asymptotic region $\eta \to \infty$ [3,5]. Tunneling occurs in the presence of the Coulomb field of the ion, and the probability to tunnel depends on its charge Z defining the power in the preexponential factor in Eq. (9). Consider an arbitrary polyatomic molecule whose nuclei are separated by sufficiently large distances. Suppose the tunneling electron is initially localized at one of the nuclei and the total charge of the resulting molecular ion is distributed among several nuclei. Then the effective charge felt by the electron varies as it moves from its *parent* nucleus to the asymptotic region, because of the charge located at the other *spectator* nuclei. The effect of this variation was not accounted for in the original development of the WFAT for compact systems [3,5]. It was included in Ref. [26], where it was shown that the distribution of the charge in the molecular ion affects the ionization rate if the distance between the parent and spectator nuclei is comparable to or larger than the width of the potential barrier through which tunneling occurs. Here, we take the effect of the spectator nucleus on tunneling ionization of H_2 into account.

We first consider the parallel geometry. In this case, tunneling preferably occurs from the lower nucleus (assuming

that the field is directed upwards); to reach the lower nucleus, the electron which is initially located near the upper nucleus must additionally tunnel between the nuclei. The lower and upper nuclei partially screened by the electron remaining in the molecular ion in the Stark-mixed state $\alpha = 1s\sigma$ are treated as parent and spectator nuclei with effective charges Z_p and Z_s, respectively. These charges must satisfy $Z_p + Z_s = Z = 1$. They can be expressed in terms of the wave function of the remaining electron. Let N_+ and N_- denote contributions to the norm of $\psi^{(1)}_{1s\sigma}(\mathbf{r}; \mathbf{R}_\parallel, F)$ from the upper ($z > 0$) and lower ($z < 0$) half-spaces, respectively, so that $N_+ + N_- = 1$. Then a sensible choice of the charges is $Z_s = 1 - N_+$ and $Z_p = 1 - N_-$. The effect of the spectator nucleus on the ionization rate is described by [26]

$$\Gamma^{\rm PS}_{1s\sigma}(\mathbf{R}_\parallel, F) = \left(\frac{RF}{2\varkappa^2}\right)^{2Z_s/\varkappa} \left(\frac{1+\zeta}{1-\zeta}\right)^{2\zeta Z_s/\varkappa} \Gamma^{\rm P}_{1s\sigma}(\mathbf{R}_\parallel, F), \tag{20}$$

where

$$\zeta = \frac{\varkappa}{(\varkappa^2 + 2RF)^{1/2}} \tag{21}$$

and $\varkappa = \varkappa_{1s\sigma}(\mathbf{R}_\parallel, F)$. We will refer to this approximation as ME-WFAT-P-S, where S stands for spectator. The *spectator* factor multiplying $\Gamma^{\rm P}_{1s\sigma}(\mathbf{R}_\parallel, F)$ in Eq. (20) turns to unity for $Z_s = 0$, as one would expect. At sufficiently small internuclear distances satisfying $RF \ll \varkappa^2$ this factor also turns to unity; in this case, the distance between the parent and spectator nuclei R is smaller than the width of the potential barrier $\sim\varkappa^2/F$, and the net effect of both nuclei is represented by the total charge of the molecular ion Z in the field factor (9). Note that there exists some ambiguity in the definition of Z_s and Z_p at small R; this, however, does not affect the rate since the spectator factor in Eq. (20) in this case is close to unity independently of the value of Z_s. In the opposite case, $RF \gg \varkappa^2$, this factor modifies $\Gamma^{\rm P}_{1s\sigma}(\mathbf{R}_\parallel, F)$ in such a way that $\Gamma^{\rm PS}_{1s\sigma}(\mathbf{R}_\parallel, F)$ coincides with the ionization rate in the presence of only the parent nucleus, with Z replaced by Z_p in Eq. (9), as if there were no spectator nucleus; for more details see Ref. [26]. Equation (20) holds uniformly in R and describes the transition between these two limits.

Before we proceed, let us reiterate the physical picture of tunneling ionization of H_2 at large R underlying Eq. (20). As one of the electrons tunnels, the other electron, remaining in the molecular ion, is redistributed between the nuclei, because the external field couples the nearly degenerate states $1s\sigma$ and $2p\sigma$ (the core polarization effect). Tunneling occurs in the presence of the Coulomb field of the parent and spectator nuclei separated by a distance R, and the ionization rate depends on how the total charge of the molecular ion is distributed among them (the spectator nucleus effect).

In the perpendicular geometry the situation is quite different, because the external field does not couple the states $1s\sigma$ and $2p\sigma$. For small R, the molecular ion remains in the Stark-mixed state $\psi^{(1)}_{1s\sigma}(\mathbf{r}; \mathbf{R}_\perp, F)$ in which the electron is equally distributed among the nuclei. However, the spectator nucleus effect in this case is small. At larger R, where the states $1s\sigma$ and $2p\sigma$ become nearly degenerate, the interelectron repulsion begins to play an important role. The electric field of an electron tunneling from one of the nuclei couples the states $1s\sigma$ and $2p\sigma$, so that the remaining electron is shifted towards the other nucleus. As a result, the charge of the spectator nucleus turns to zero as R grows, and the effect disappears. This scenario is confirmed by *ab initio* calculations [15] discussed in Sec. IV. We thus conclude that the spectator nucleus effect for H_2 in the perpendicular geometry is small and can be neglected.

D. Internuclear motion effect

So far we assumed that the nuclei in H_2 are frozen. The importance of the effect of the internuclear motion on the ionization rate is demonstrated by a recent observation of the isotope effect in strong-field ionization of hydrogen molecules [28]. We take this effect into account following Ref. [27]. The ground vibrational state describing the internuclear motion in H_2 in the Born-Oppenheimer (BO) approximation is defined by

$$\left[-\frac{1}{M}\frac{d^2}{dR^2} + \frac{1}{R} + E^{(2)}_0(\mathbf{R}, F) - E_0(\beta, F)\right]\chi_0(\mathbf{R}, F) = 0, \tag{22}$$

where M is the nuclear mass. In the presence of an external field, the electronic energy $E^{(2)}_0(\mathbf{R}, F)$ in Eq. (22) becomes complex [5,14,44], and its imaginary part determines the ionization rate at fixed $\mathbf{R}$ discussed above. The total energy of the molecule $E_0(\beta, F)$ also becomes complex, and its imaginary part defines the ionization rate of the molecule including the internuclear motion. In the weak-field limit, $F \to 0$, the electronic energy can be substituted from Eq. (12) and the latter rate can be obtained using perturbation theory as the expectation value of the former rate in the state $\chi_0(\mathbf{R}, F)$. In the parallel geometry, we average the ME-WFAT-P-S rate given by Eq. (20),

$$\Gamma^{\rm PSN}_{1s\sigma,\parallel}(F) = \int_0^\infty \Gamma^{\rm PS}_{1s\sigma}(\mathbf{R}_\parallel, F)\chi_0^2(\mathbf{R}_\parallel, F)\, dR. \tag{23}$$

We will refer to this approximation as ME-WFAT-P-S-N, where N stands for nuclear. In the perpendicular geometry the spectator nucleus effect is neglected, so we average the ME-WFAT-P rate given by Eq. (17) with $\alpha = 1s\sigma$,

$$\Gamma^{\rm PN}_{1s\sigma,\perp}(F) = \int_0^\infty \Gamma^{\rm P}_{1s\sigma}(\mathbf{R}_\perp, F)\chi_0^2(\mathbf{R}_\perp, F)\, dR. \tag{24}$$

We include only the internuclear motion, assuming that the molecule is sharply aligned. The effect of the rotational motion on the ionization rate of H_2 in the ground rotational state was discussed in Ref. [45].

III. NUMERICAL IMPLEMENTATION

In this section, we outline the implementation of the theory in the present calculations. The fully correlated two-electron wave function is constructed by solving Eq. (1) using the method and program described in Ref. [46]. We use the symmetric James-Coolidge basis with the sum of the powers of interparticle distances less or equal to 16 (the parameter Ω in Ref. [46]). The nonlinear parameter of the basis is chosen to minimize the two-electron energy $E^{(2)}_0(R)$ at each R. The field-free BO potential for H_2 is shown by the lowest (black)

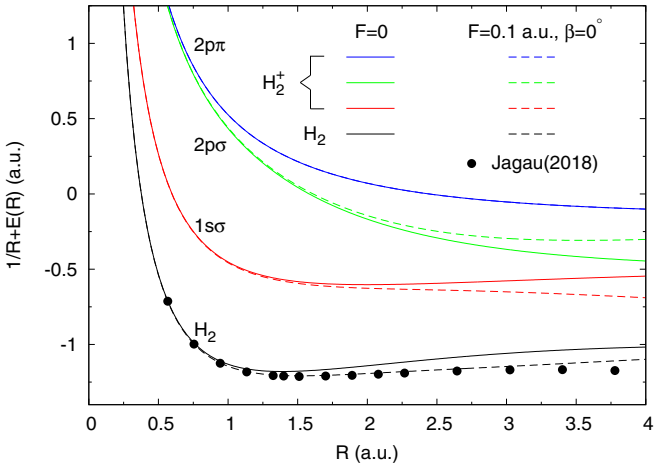

FIG. 1. BO potentials for H_2 and H_2^+ at $F = 0$ (solid lines) and $F = 0.1$ at $\beta = 0^\circ$ (dashed lines). The electronic energy $E(R)$ for H_2 at $F = 0$ is equal to $E_0^{(2)}(R)$ defined by Eq. (1); at $F = 0.1$ it is equal to $E_0^{(2)}(\mathbf{R}_\parallel, F)$ defined by Eq. (12). Solid circles show the corresponding potential obtained using the *ab initio* electronic energy from Ref. [15]. The electronic energy $E(R)$ for H_2^+ at $F = 0$ is equal to $E_n^{(1)}(R)$ defined by Eq. (3); at $F = 0.1$ it is equal to $E_\alpha^{(1)}(\mathbf{R}_\parallel, F)$ defined by Eq. (14). Only the three lowest states of H_2^+ shown are coupled in Eq. (14) in the present calculations. For $\beta = 0^\circ$, the $2p\pi$ state is decoupled from the other two states, so the solid and dashed lines for this state coincide.

solid line in Fig. 1. It has a minimum at the equilibrium internuclear distance $R_0 = 1.4011$ [47]. The one-electron wave functions are obtained by solving Eq. (3) in prolate spheroidal coordinates using discrete variable representations based on Jacobi and Laguerre polynomials [48], as in Ref. [17]. The field-free BO potentials for the three lowest states of H_2^+ are shown in Fig. 1 by solid lines labeled by the state. The wave functions are then used to calculate Dyson orbitals (4).

The structure factors (7) are calculated using an approach introduced in Ref. [19]. The structure function (8) at $\eta \to \infty$ can be expanded in powers of $1/\eta$,

$$G_n(\eta; \mathbf{R})|_{\eta\to\infty} = G_n(\mathbf{R}) + \sum_{k=1}^{N_{\rm fit}} \frac{C_k^{(n)}(\mathbf{R})}{\eta^k}. \qquad (25)$$

The numerical results obtained from Eq. (8) are fitted by this equation, which yields $G_n(\mathbf{R})$. The interval of η used in the fitting procedure is found as follows. Although both two- and one-electron wave functions used in the present calculations are highly accurate in the region of their localization, they become less accurate in the asymptotic region, and therefore so do Dyson orbitals (4). This is a common problem of wave functions obtained by the variational method, when nonlinear parameters defining exponential factors in the basis functions are chosen to minimize the energy of the state, disregarding its asymptotic behavior. For any finite basis, such wave functions have correct asymptotic behavior only in a finite region of space. By varying different parameters of the numerical scheme it is possible to determine the upper boundary $\eta_{\rm max}$ of the interval of η where Eq. (8) yields stable results. On the other hand, the lower boundary $\eta_{\rm min}$ of the interval where Eq. (25) holds for a given $N_{\rm fit}$ can be determined by requiring

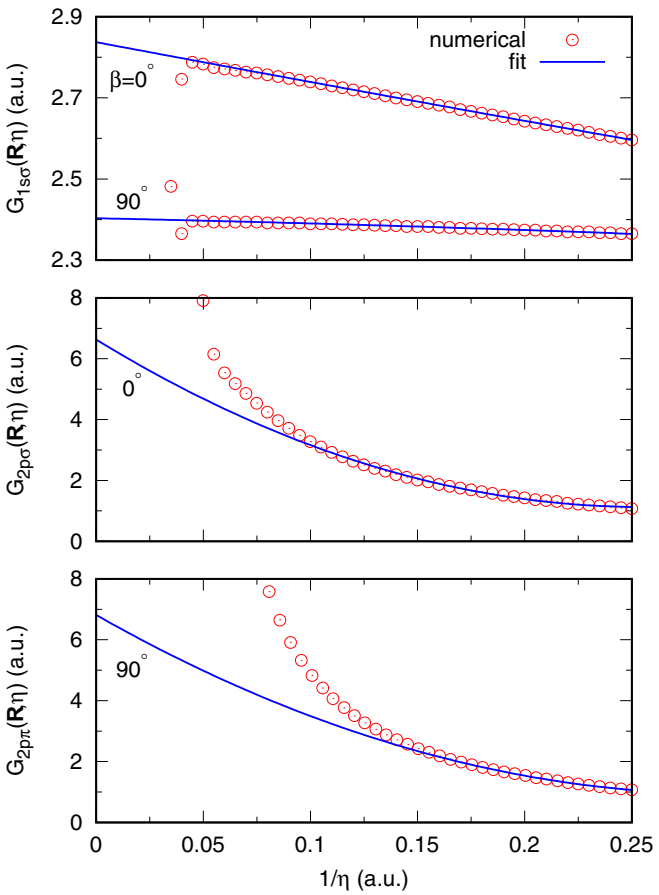

FIG. 2. Illustration of the fitting procedure used to calculate structure factors. Open circles show structure functions for three states of H_2^+ at $R = 1.4$ calculated using Eq. (8). Solid lines show fits to the numerical results by Eq. (25). The fitting intervals are discussed in the paper.

that the fit should satisfy a certain accuracy criterion. This defines the fitting interval $\eta_{\rm min} < \eta < \eta_{\rm max}$. The procedure is rather accurate, provided that $\eta_{\rm max}$ is sufficiently large. The same procedure was used in systematic calculations of structure factors for diatomic molecules in the Hartree-Fock approximation [18] and in the configuration-interaction calculations for H_2 and LiH [33].

To illustrate the procedure, we discuss the calculation of $G_n(\mathbf{R})$ for the three states of H_2^+ shown in Fig. 1 at $R = 1.4$. The $2p\pi$ state is represented by a real function which behaves as $\psi_{2p\pi}^{(1)}(\mathbf{r}; \mathbf{R}_\parallel) \propto \cos\varphi$. The phases of the functions $\psi_n^{(1)}(\mathbf{r}; \mathbf{R})$ are chosen such that all $G_n(\mathbf{R})$ are positive. The factor $G_{1s\sigma}(\mathbf{R})$ is calculated for both parallel and perpendicular geometries. The $2p\sigma$ state is considered only in the parallel geometry and the $2p\pi$ state is considered only in the perpendicular geometry; the corresponding Dyson orbitals for $\beta = 90^\circ$ and 0°, respectively, turn to zero along the z axis, so $G_{2p\sigma}(\mathbf{R}_\perp) = G_{2p\pi}(\mathbf{R}_\parallel) = 0$. The open circles in Fig. 2 show structure functions calculated using Eq. (8). The solid lines show fits to the results by Eq. (25). For the $1s\sigma$ state at both orientations, the structure function can be reliably calculated in a rather wide interval of η. In the fitting procedure we use the interval $0.125 < 1/\eta < 0.25$, and the fit is seen to

TABLE I. Structure factors (7) calculated using Dyson orbitals (4) for the three lowest field-free states of H_2^+ in the parallel and perpendicular geometries for a set of internuclear distances R, including the equilibrium distance $R_0 = 1.4011$ for H_2. Note that $G_{2p\sigma}(\mathbf{R}_\perp) = G_{2p\pi}(\mathbf{R}_\parallel) = 0$, because of the symmetry of the states.

R	$G_{1s\sigma}(\mathbf{R}_\parallel)$	$G_{1s\sigma}(\mathbf{R}_\perp)$	$G_{2p\sigma}(\mathbf{R}_\parallel)$	$G_{2p\pi}(\mathbf{R}_\perp)$
0.75	2.82	2.67	8.8	7.9
1.00	2.81	2.56	8.0	7.5
1.25	2.82	2.46	7.2	7.1
1.4011	2.83	2.40	6.6	6.8
1.50	2.86	2.37	6.3	6.6
1.75	2.93	2.29	5.6	6.2
2.00	3.02	2.22	5.0	5.8
2.25	3.13	2.15	4.6	5.4
2.50	3.28	2.10	4.3	5.0
2.75	3.45	2.05	4.1	4.6
3.00	3.63	2.01	4.1	4.2
3.25	3.82	1.98	4.1	3.8
3.50	4.02	1.94	4.2	3.5

well reproduce the numerical results up to $1/\eta = 0.05$. In this case, fitting is performed with $N_{\rm fit} = 3$; the inclusion of higher-order terms in Eq. (25) does not change the results for $G_{1s\sigma}(\mathbf{R})$ within 1%. For the $2p\sigma$ state the results from Eq. (8) become unstable at a smaller $\eta_{\rm max}$. In this case, we use the same fitting interval $0.125 < 1/\eta < 0.25$, but with $N_{\rm fit} = 2$. The numerical results begin to depart from the fit already at $1/\eta = 0.1$. The departure is caused by inaccuracy of the structure function, which is a consequence of the inaccuracy of two- and one-electron wave functions in the asymptotic region. The increase of $N_{\rm fit}$ in this case does not improve the results, because the fit tends to reproduce the rising part of the structure function at smaller $1/\eta$, where it is inaccurate. For the $2p\pi$ state the situation becomes worse. In this case $\eta_{\rm max}$ is even smaller, and we use a narrower fitting interval $0.17 < 1/\eta < 0.25$ with $N_{\rm fit} = 2$. The limited accuracy of the present wave functions restricts our calculations to the three states considered. To extend the calculations by the present method to higher states wave functions with more accurate asymptotic tails are needed. We mention that this difficulty can be resolved by using the integral representation for structure factors [49], which, however, has so far been implemented only within the Hartree-Fock approximation [20,21].

The calculations yield four structure factors discussed above as functions of R. For reference purposes, we present the results for a set of internuclear distances in Table I. The results for the $1s\sigma$ state are rather accurate, we estimate that the error is of the order of unity in the last digit quoted. These results can be compared with previous calculations. The factor $G_{1s\sigma}(\mathbf{R}_\parallel)$ at $R = R_0$ was for the first time evaluated using a variational two-electron wave function in Ref. [5]. The result obtained therein 2.73 is slightly smaller than the present result. In the present calculations we used a more accurate two-electron wave function, so we are sure that the present result is more accurate. The factor $G_{1s\sigma}(\mathbf{R})$ as a function of β at $R = R_0$ was calculated by the time-dependent generalized-active-space configuration-interaction method in Ref. [33] [the factor $G_{000}(\beta)$ for H_2 in this paper in the present notation coincides with $G_{1s\sigma}(\mathbf{R})/\sqrt{2}$ at $R = R_0$]. The results obtained in the most accurate set of calculations therein denoted by CAS*(2,160)-1 are 2.82 and 2.41 for $\beta = 0^\circ$ and 90°, respectively, which is very close to the present results. This level of agreement confirms high accuracy of both calculations. It is worthwhile to mention that the same structure factors calculated in the Hartree-Fock approximation are 1.91 and 1.66, respectively [17,18]; the difference characterizes the role of the interelectron correlation effects. The present results for the other two states are less accurate, so we give them with only two significant digits in Table I. We are not aware of any other calculations of these structure factors.

The polarizabilities $\alpha(\mathbf{R}_\parallel)$ and $\alpha(\mathbf{R}_\perp)$ of H_2 needed to evaluate the Stark shift of the initial state are taken from Ref. [50]. The BO potential for H_2 including the Stark shift calculated using Eq. (12) at $F = 0.1$ and $\beta = 0^\circ$ is shown by the lowest (black) dashed line in Fig. 1. The solid circles show the results obtained using the *ab initio* electronic energy from Ref. [15]. The relative error of Eq. (12) as compared to the *ab initio* results [15] depends on F and R. For $F = 0.1$ in the interval $R < 3.5$, which is sufficient to describe the experiments [29,30], the error grows with R but remains less than 3.4% and 0.77% for $\beta = 0^\circ$ and 90°, respectively.

The Stark-mixed states of H_2^+ are constructed by solving Eq. (14). We include all three field-free states discussed above in the expansion (13). In the parallel geometry, the field couples the $1s\sigma$ and $2p\sigma$ states, while the $2p\pi$ state is decoupled. The Stark-shifted BO potentials for H_2^+ in this case at $F = 0.1$ are shown by dashed lines in Fig. 1. On the other hand, in the perpendicular geometry, the $1s\sigma$ and $2p\pi$ states are coupled, while the $2p\sigma$ state is decoupled. Thus, we include the two lowest coupled states in Eq. (13) for both geometries.

Figure 3 illustrates the structure of the Stark-mixed state $1s\sigma$ of H_2^+ in the parallel geometry for $F = 0.1$ at two internuclear distances. This state is distorted compared to the corresponding field-free state which is symmetric with respect to the (x, y) plane. The electron in this state is shifted by the field towards the lower nucleus, and the polarization grows with R. Figure 4 shows the corresponding Stark-mixed Dyson orbital calculated for the same field strength and internuclear distances. This orbital is also distorted compared to the field-free case, when it is symmetric with respect to the (x, y) plane, but its center of gravity is shifted in the opposite direction, towards the upper nucleus. Such a behavior of the Stark-mixed Dyson orbital is crucial for understanding the role of the core polarization effect in the results discussed below.

The ground-state solution to Eq. (22) for H_2 with $M = m_p$, where $m_p = 1836$ is the proton mass, is illustrated in Fig. 5. The field-free wave function is localized near the equilibrium internuclear distance R_0. The maximum of the field-distorted wave function calculated for the same $F = 0.1$ and $\beta = 0^\circ$ as in Fig. 1 is shifted towards larger R, following the minimum of the Stark-shifted BO potential. We also show the integrand in Eq. (23). The energy difference in Eq. (19), which has the meaning of the ionization potential, decreases as R grows, so the rate $\Gamma^{\rm PS}_{1s\sigma}(\mathbf{R}_\parallel, F)$ increases. As a result, the maximum of the integrand in Eq. (23) is shifted towards larger R with respect to the maximum of the nuclear wave function. The shift depends on the nuclear mass defining the width of the

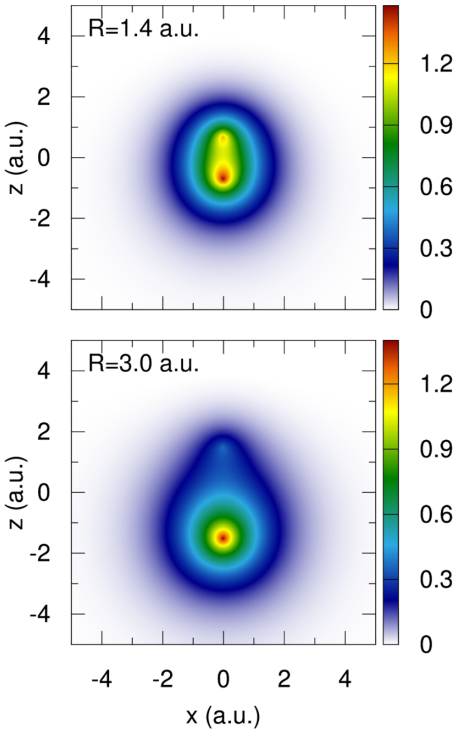

FIG. 3. The Stark-mixed state $\alpha = 1s\sigma$ of H_2^+ [see Eqs. (13) and (14)] for $\beta = 0^\circ$ and $F = 0.1$ at two internuclear distances R indicated in the figure. The state is axially symmetric about the z axis, its cuts by the (x, z) plane are shown.

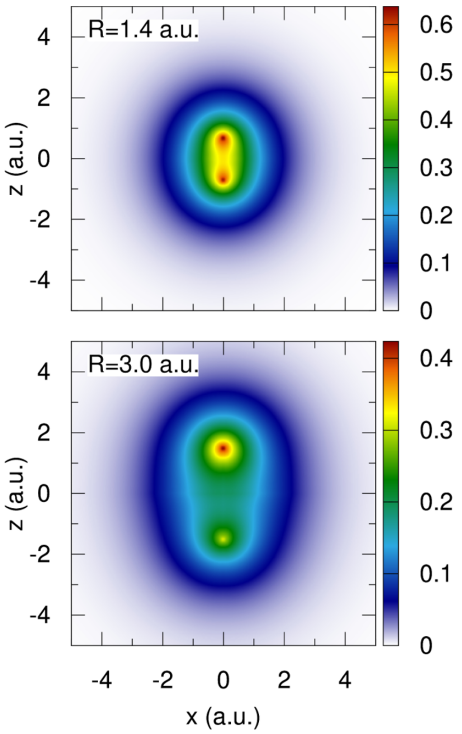

FIG. 4. The Stark-mixed Dyson orbital $\alpha = 1s\sigma$ [see Eq. (16)] for the same $\beta = 0^\circ$, $F = 0.1$, and two internuclear distances R as in Fig. 3.

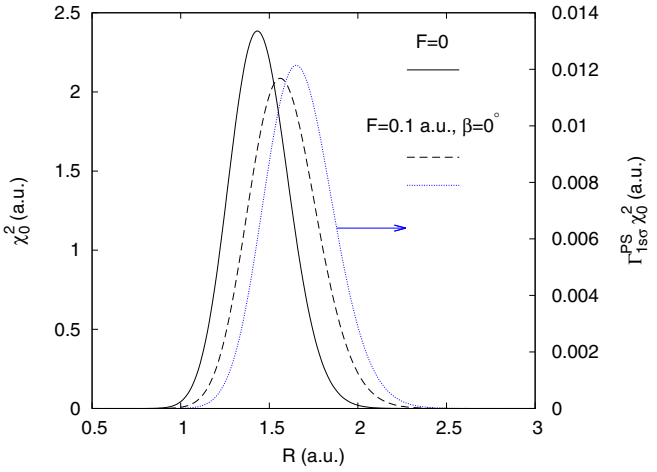

FIG. 5. The nuclear wave function $\chi_0(\mathbf{R}_\parallel, F)$ squared in the ground state of H_2 obtained by solving Eq. (22) for $F = 0$ (solid line) and $F = 0.1$ at $\beta = 0^\circ$ (dashed line). The corresponding BO potentials are shown in Fig. 1. The dotted line (right axis) shows the integrand in Eq. (23).

wave function, which explains the isotope effect in tunneling ionization of molecules predicted in Ref. [27] and observed in Ref. [28].

IV. RESULTS AND DISCUSSION

In this section, we compare the theory with benchmark theoretical and experimental results. The goal of the comparison is to explore how the inclusion of the effects discussed above affects the ionization rate.

A. Comparison with *ab initio* calculations

Early *ab initio* calculations of the ionization rate of H_2 with frozen nuclei in the parallel geometry were performed in Refs. [14,51,52]. Recently, more extensive calculations for a set of internuclear distances and field strengths in both parallel and perpendicular geometries have been reported [15]. We use these results to gauge the different approximations of the theory for fixed $\mathbf{R}$ discussed in Sec. II.

Figures 6 and 7 show ionization rates for the parallel and perpendicular geometries, respectively, as functions of the field strength at three internuclear distances. Lines in the figures show the present results and circles show the *ab initio* results from Ref. [15]. In addition, crosses in Fig. 6 show the *ab initio* results from Ref. [14]. The ME-WFAT-P-S results are not shown in Fig. 7, because we do not include the spectator nucleus effect in the perpendicular geometry. To facilitate comparison of the different results on a linear scale, all the rates shown in the figures are divided by the same field factor $W(F, \varkappa_{1s\sigma}(R))$ defined by Eqs. (9) and (10). Let us discuss the different approximations separately.

Within the leading-order approximation ME-WFAT(0), the ratio shown in Figs. 6 and 7 does not depend on F and is given by the structure factor squared $G^2_{1s\sigma}(\mathbf{R})$ for the corresponding $\mathbf{R}$. According to the ME-WFAT [5], this is the limiting value of the ratio for $F \to 0$. We note that *ab initio* calculations become problematic at sufficiently weak fields, where the

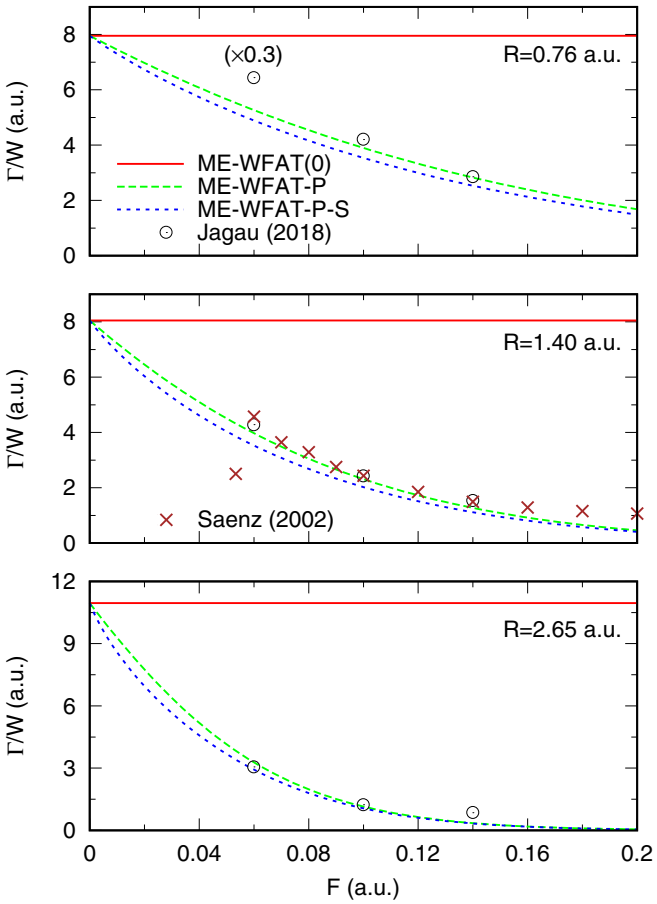

FIG. 6. Ionization rates of H_2 with frozen nuclei at three internuclear distances R in the parallel geometry ($\beta = 0^\circ$) as functions of the field strength F. Solid (red), dashed (green), and short-dashed (blue) lines show the rates $\Gamma^{(0)}_{1s\sigma}(\mathbf{R}_\parallel, F)$, $\Gamma^{\rm P}_{1s\sigma}(\mathbf{R}_\parallel, F)$, and $\Gamma^{\rm PS}_{1s\sigma}(\mathbf{R}_\parallel, F)$ defined by Eqs. (6), (17), and (20), respectively. Circles and crosses show *ab initio* results from Refs. [15] and [14], respectively. In the top panel, the rate at $F = 0.06$ from Ref. [15] is multiplied by 0.3, to bring its value to the scale of the figure. All the rates are divided by the same field factor $W(F, \varkappa_{1s\sigma}(R))$ defined by Eqs. (9) and (10).

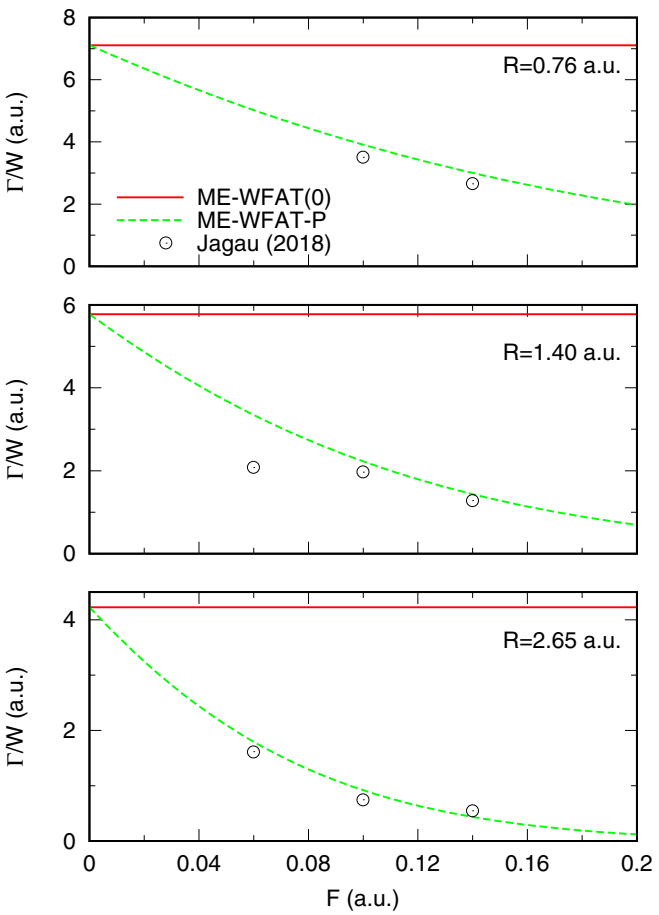

FIG. 7. Same as in Fig. 6, but for the perpendicular geometry ($\beta = 90^\circ$). Solid (red) and dashed (green) lines show the rates $\Gamma^{(0)}_{1s\sigma}(\mathbf{R}_\perp, F)$ and $\Gamma^{\rm P}_{1s\sigma}(\mathbf{R}_\perp, F)$, respectively. Circles show *ab initio* results from Ref. [15].

rate is too small. In particular, this is the reason why the calculations in Refs. [14,15] were not extended to weaker fields. Furthermore, at the weakest field where the results are reported they may be not so accurate. Thus, in the top panel of Fig. 6, the rate at $F = 0.06$ from Ref. [15] is multiplied by 0.3, to bring its value to the scale of the figure; this, in our opinion, indicates that the result is inaccurate. In the middle panel of Fig. 6, there is a visible difference between the rates at $F = 0.06$ from Refs. [14] and [15], although at stronger fields the results of the two calculations closely agree with each other. In the same panel, the rate at the weakest field from Ref. [14] is smaller than what is expected by extrapolating the results from stronger fields, which also indicates its inaccuracy. Anyway, visual extrapolation of the *ab initio* results to $F = 0$ is consistent with the value $G^2_{1s\sigma}(\mathbf{R})$ predicted by ME-WFAT(0). This is probably not so evident in Fig. 7, where only few *ab initio* points in F are available, but this is rather clearly seen in the middle panel in Fig. 6, where the dependence on F is presented in more detail. This is a typical pattern of convergence of *ab initio* results to WFAT results at $F \to 0$ similar to that seen previously for other systems [4,6,8]. We note, however, that more accurate *ab initio* calculations at weaker fields are needed to unambiguously confirm the convergence for H_2. The critical field $F_c(R)$ estimated from Eq. (11) is equal to 0.34, 0.21, and 0.12 at $R = 0.76$, 1.40 and 2.65, respectively. Thus, for a given F, the condition $F \ll F_c(R)$ is better fulfilled for smaller R. Indeed, the *ab initio* results in Figs. 6 and 7 lie closer to the ME-WFAT(0) results for $R = 0.76$ than for $R = 2.65$.

The Stark-shift and core polarization effects included in ME-WFAT-P make the ratio shown in Figs. 6 and 7 dependent on F. This essentially improves the present results, bringing them in good agreement with the *ab initio* results. The difference between the ME-WFAT(0) and ME-WFAT-P rates can be understood by comparing Eq. (6) for $n = 1s\sigma$ with Eq. (17) for $\alpha = 1s\sigma$. Both factors in Eq. (17) are changed compared to Eq. (6). The field factor is changed because the ionization potential is changed. Note that Stark shifts of the initial and final states are both negative (see Fig. 1), so they partially compensate each other in Eq. (19). For all values of R and F shown in the figures we have $I_{1s\sigma}(\mathbf{R}, F) > I_{1s\sigma}(R)$, i.e., the Stark shift increases the ionization potential. As a result, the field factor in Eq. (17) is smaller than that in Eq. (6), because

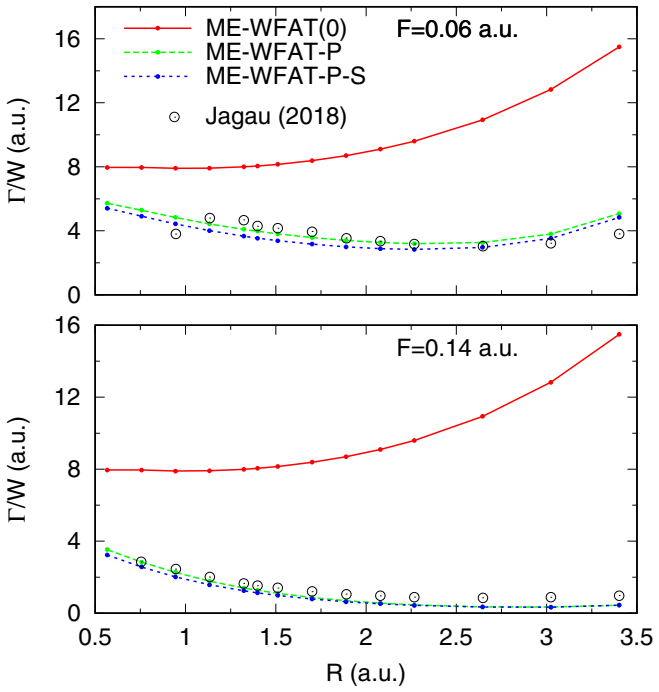

FIG. 8. Similar to Fig. 6, but the rates are shown as functions of the internuclear distance R in the parallel geometry ($\beta = 0^\circ$) at two field strengths F. Solid (red), dashed (green), and short-dashed (blue) lines show the rates $\Gamma^{(0)}_{1s\sigma}(\mathbf{R}_\parallel, F)$, $\Gamma^{\mathrm{P}}_{1s\sigma}(\mathbf{R}_\parallel, F)$, and $\Gamma^{\mathrm{PS}}_{1s\sigma}(\mathbf{R}_\parallel, F)$, respectively. Circles show *ab initio* results from Ref. [15]. All the rates are divided by the same field factor $W(F, \varkappa_{1s\sigma}(R))$.

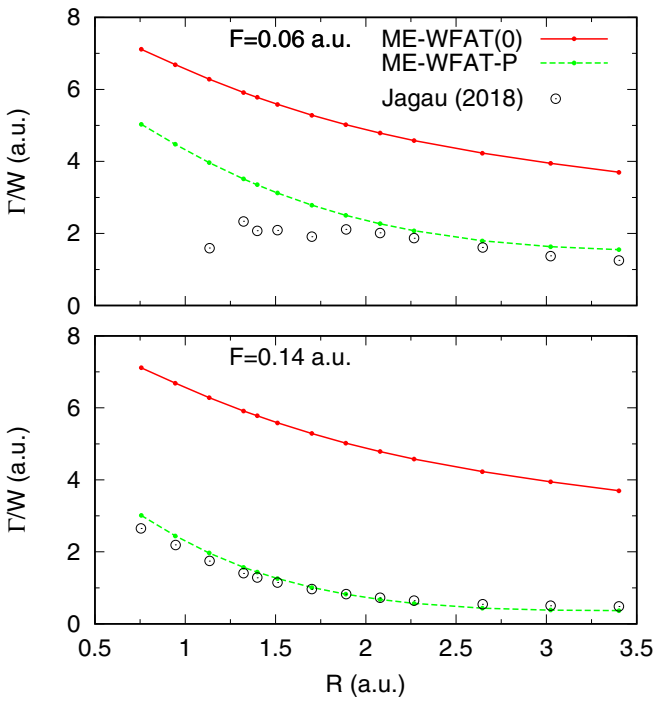

FIG. 9. Same as in Fig. 8, but for the perpendicular geometry ($\beta = 90^\circ$). Solid (red) and dashed (green) lines show the rates $\Gamma^{(0)}_{1s\sigma}(\mathbf{R}_\perp, F)$ and $\Gamma^{\mathrm{P}}_{1s\sigma}(\mathbf{R}_\perp, F)$, respectively. Circles show *ab initio* results from Ref. [15].

of the exponential factor in Eq. (9). The structure factor in Eq. (17) is also smaller than that in Eq. (6), because of the distortion of the Stark-mixed Dyson orbital (see Fig. 4) caused by the core polarization effect. Thus, both factors in Eq. (17) are decreased, which explains the decrease of the rate. It is instructive to quantify the effects. Consider, for example, the situation for $\beta = 0^\circ$ and $R = 1.4$ at $F = 0.1$; see the middle panel in Fig. 6. In this case, the structure and field factors in Eq. (17) are smaller than the corresponding factors in Eq. (6) by factors of 0.50 and 0.57, respectively. This shows that both the Stark-shift and core polarization effects play an important role in achieving good agreement with the *ab initio* results, which is one of the physical insights resulting from the present theory.

The inclusion of the spectator nucleus effect in ME-WFAT-P-S only slightly modifies the rates in Fig. 6. The difference between the ME-WFAT-P and ME-WFAT-P-S rates is described by the spectator factor in Eq. (20). For any fixed R, this factor turns to unity at $F \to 0$. It remains close to unity for all values of R and F shown in the figure. We will see, however, that even the small (∼10%) difference between the rates produces an appreciable effect on the anisotropy ratio.

Figures 8 and 9 show similar comparison, but now the rates are plotted as functions of the internuclear distance at two field strengths. The rates are again divided by the same field factor $W(F, \varkappa_{1s\sigma}(R))$. Some irregularity in the behavior of the *ab initio* results for $F = 0.06$ in the interval $1 < R < 2$ reflects the computational problem mentioned above. For $R \to 0$, the system becomes isotropic and the rates in the parallel and perpendicular geometries coincide. All the calculations predict that at nonzero R the molecule is more easily ionized in the parallel geometry; this anisotropy of the ionization rate is discussed in the next section. Similar to the situation seen in Figs. 6 and 7, the ME-WFAT-P rates are essentially closer to the *ab initio* results than the ME-WFAT(0) rates. The ME-WFAT-P-S rates in Fig. 8 only slightly differ from the ME-WFAT-P rates, as in Fig. 6. Notice that the *ab initio* results in the top panel of Fig. 8 begin to grow with R at $R > 2.5$, and this growth is reflected in the present results. The critical field $F_c(R)$ monotonically decreases from 0.44 to 0.11 as R grows from 0.5 to 3.5. Thus, in the top panels of Figs. 8 and 9 F remains smaller than $F_c(R)$ for all R. The condition (11) is better fulfilled at smaller R, where the ME-WFAT(0) results indeed lie closer to the *ab initio* results. In the bottom panels, F becomes larger than $F_c(R)$ at $R > 2.2$. The WFAT does not apply in this case, of course. We nevertheless show these results for completeness of the presentation.

Summarizing, our calculations demonstrate that the inclusion of the Stark shift and core polarization effects on the basis of the leading-order theory ME-WFAT(0) essentially improves the results and yields the ionization rate of H_2 with frozen nuclei in good agreement with the *ab initio* results. This confirms the physical picture underlying the present treatment of the effects. The spectator nucleus effect, on the other hand, only weakly affects the rates. The remaining difference between the present results and the *ab initio* results is caused by the distortion of the initial state of H_2, contribution to the core polarization effect from higher excited states of H_2^+, as well as higher-order terms in the asymptotic expansion in F not included in the present theory. We emphasize that all

the reasons causing the difference disappear at $F \to 0$ and ME-WFAT(0) becomes exact in this limit.

Let us return to the discussion in the end of Sec. II C. The ionization rate of H_2 at $\beta = 90^\circ$, $R = 4$ Å ($\approx$7.6 a.u.), and $F = 0.06$ is $\Gamma_\perp(H_2) = 1.026\times10^{-3}$ [15]. Meanwhile, the ionization rate of the hydrogen atom at the same field is $\Gamma(H) = 0.5151\times10^{-3}$ [4]. Thus, $2\Gamma(H) = 1.030\times10^{-3}$, which is very close to $\Gamma_\perp(H_2)$. This means that the ionization of H_2 at sufficiently large R in the perpendicular geometry proceeds as ionization of two independent neutral hydrogen atoms. The applicability of such an independent atom model in this case supports our neglect of the spectator nucleus effect in the perpendicular geometry, because the spectator has zero charge. Note that at $\beta = 0^\circ$ and the same R and F the ionization rate of H_2 is $\Gamma_\parallel(H_2) = 98.86\times10^{-3}$ [15], which is 96 times larger than $\Gamma_\perp(H_2)$. Thus, the independent atom model completely fails in the parallel geometry, and the reason of the failure roots in the large Stark shift and polarization of the final state.

B. Comparison with experiments

Experimental studies of strong-field ionization of molecules by circularly polarized laser pulses in the adiabatic regime provide unbiased access to the ionization rate in a static electric field [2]. Usually, absolute values of the rate are not measured, but there are many accurate relative measurements characterizing its dependence on the orientation of the molecule and field strength [28–30,53–55]. In particular, in Ref. [29] the ratio of the ionization yields for H_2 in the parallel and perpendicular geometries was measured. Soon after that, in Ref. [30], the same anisotropy ratio was measured for D_2. We use these experimental results to illustrate the predictive power of the present theory. In addition, we analyze the relative importance of the different effects discussed above.

The results of our calculations and the experimental results from Refs. [29,30] are presented in Fig. 10. The anisotropy ratio is shown as a function of the field strength F. One should distinguish between the ionization rate at a given F and the ionization yield—the total probability of ionization by a particular laser pulse with amplitude F. We begin with discussing the anisotropy ratio of *rates*. However, to compare with experiments, we will eventually have to turn to the anisotropy ratio of *yields*. The difference between the two ratios is caused by the variation of the laser field with time and depletion.

Most of the present results in Fig. 10 (except the thick solid lines indicated by $Y_\parallel/Y_\perp$) show the anisotropy ratio of ionization rates, $\Gamma_\parallel/\Gamma_\perp$. The different lines are calculated using different rates. The WFAT-HF, ME-WFAT(0), ME-WFAT-P, and ME-WFAT-P-S results are obtained for a fixed R equal to the equilibrium internuclear distance R_0. The ME-WFAT-P-S-N results include the internuclear motion effect and hence are different for H_2 and D_2. Below we discuss the results separately, starting from the basic leading-order theory and successively including the different effects.

The ME-WFAT(0) result for the ratio is $\Gamma^{(0)}_{1s\sigma}(\mathbf{R}_\parallel, F)/\Gamma^{(0)}_{1s\sigma}(\mathbf{R}_\perp, F) = G^2_{1s\sigma}(\mathbf{R}_\parallel)/G^2_{1s\sigma}(\mathbf{R}_\perp)$ calculated at $R = R_0$. The field factor in Eq. (6) is canceled, so the ratio is determined by the structure factors for the field-free Dyson orbital $n = 1s\sigma$. This gives a constant 1.39; see Table I. Using the structure factors from Ref. [33], the ratio is 1.37; the small difference between the results is consistent with the 1% accuracy of the present structure factors. This is the exact value of the anisotropy ratio of rates at $R = R_0$ for $F \to 0$. This approximation overestimates the ratio and does not reproduce its dependence on F. Note that ME-WFAT(0) used in Sec. II as the starting point of the present theory already includes interelectron correlation effects represented by the exact two-electron energy of the initial state in Eq. (10) and the exact structure factor in Eq. (6). The role of correlation effects can be evaluated by comparing the ME-WFAT(0) results with the WFAT-HF results obtained in the Hartree-Fock approximation [17,18]. We have not discussed this comparison in the pre-

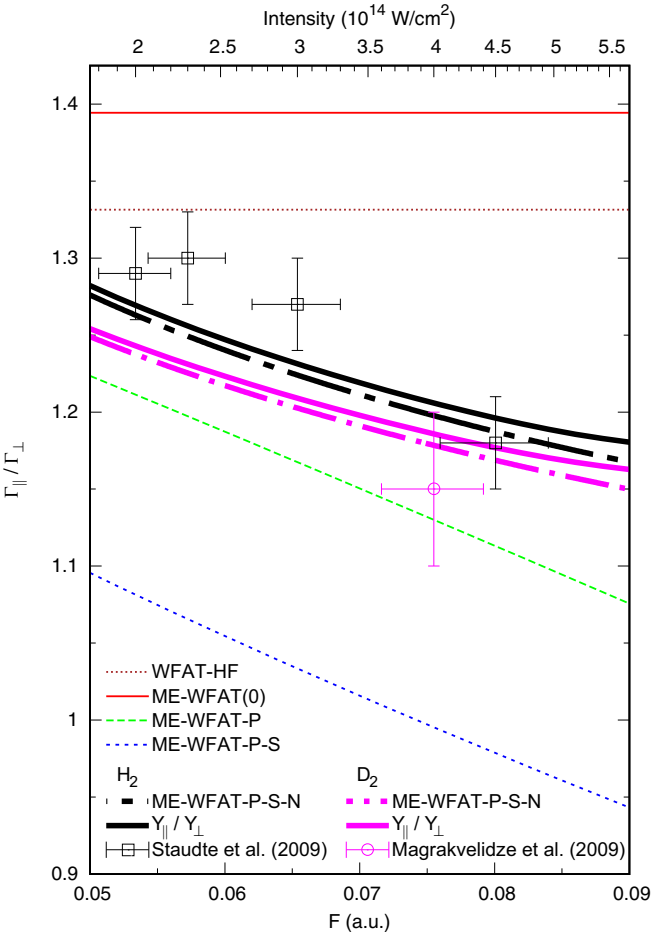

FIG. 10. Ratio of the ionization rates in the parallel ($\beta = 0^\circ$) and perpendicular ($\beta = 90^\circ$) geometries as a function of the field strength F. The WFAT-HF, ME-WFAT(0), ME-WFAT-P, and ME-WFAT-P-S results are obtained for the equilibrium internuclear distance $R_0 = 1.4011$. The ME-WFAT-P-S-N results shown by the upper and lower thick dashed-dotted lines include the internuclear motion effect for H_2 and D_2, respectively. The corresponding upper and lower solid lines indicated by $Y_\parallel/Y_\perp$ show the ratios of ionization yields for H_2 and D_2 obtained from Eq. (31) for pulses used in Refs. [29] and [30], respectively. Symbols with error bars show experimental results for H_2 [29] and D_2 [30]. The top axis shows the intensity $I = cF^2/4\pi$ of a circularly polarized laser field with amplitude F.

vious sections, because the absolute value of the ionization rate is very sensitive to the ionization potential, which causes a large difference between the ME-WFAT(0) and WFAT-HF rates. However, in the ratio shown in Fig. 10 the field factor, which is most sensitive to the ionization potential, is canceled, so we can compare the results on a linear scale. The WFAT-HF result for the ratio is 1.33 [17,18]; it is also shown in Fig. 10. Interestingly, the step from WFAT-HF to ME-WFAT(0), that is, the inclusion of correlation effects shifts the results farther from the experiment.

The ME-WFAT-P results are given by $\Gamma^{\rm P}_{1s\sigma}(\mathbf{R}_\parallel, F)/\Gamma^{\rm P}_{1s\sigma}(\mathbf{R}_\perp, F)$ calculated at $R = R_0$. In this approximation, the ratio is considerably decreased and slightly underestimates the experimental results. Furthermore, it becomes dependent on F, because the structure factor for the Stark-mixed Dyson orbital $\alpha = 1s\sigma$ in Eq. (17) depends on F and the field factor is not fully canceled anymore. The ME-WFAT-P results reproduce the fact that the ratio decreases as F grows, and the rate of the decrease is close to that in the experimental results. Thus, the inclusion of the Stark-shift and core-polarization effects makes both the absolute value of the ratio and its dependence on F closer to the experimental results.

The ME-WFAT-P-S results are given by $\Gamma^{\rm PS}_{1s\sigma}(\mathbf{R}_\parallel, F)/\Gamma^{\rm P}_{1s\sigma}(\mathbf{R}_\perp, F)$ calculated at $R = R_0$. The difference from the ME-WFAT-P results stems from the spectator factor in Eq. (20). Remarkably, the step from ME-WFAT-P to ME-WFAT-P-S, that is, the inclusion of the spectator nucleus effect, which resulted in only a small change of the rates in Figs. 6 and 8, produces a rather strong effect on the anisotropy ratio of rates. In this approximation, the ratio is decreased by about 10%, which is consistent with the decrease of the rates in Figs. 6 and 8. This shifts the ratio farther from the experimental results. At the same time, the slope of its dependence on F remains almost unchanged and close to that in the experiment.

So far, we discussed rates calculated at $R = R_0$. We now include the internuclear motion effect. The ME-WFAT-P-S-N results are given by $\Gamma^{\rm PSN}_{1s\sigma,\parallel}(F)/\Gamma^{\rm PN}_{1s\sigma,\perp}(F)$ calculated using Eqs. (23) and (24). They depend on the nuclear mass M appearing in Eq. (22) and are shown for both H_2 ($M = m_p$) and D_2 ($M = 2m_p$). The step from ME-WFAT-P-S to ME-WFAT-P-S-N leads to a considerable increase of the ratio and a slight decrease of the slope of its dependence on F. As a result, the ME-WFAT-P-S-N results lie close to the experimental results and reproduce their dependence on F. This approximation presents our final results for the anisotropy ratio of rates. We emphasize that all the effects mentioned in the title should be taken into account in order to achieve this level of agreement.

As yet another example of physical insight resulting from the present theory, let us discuss the isotope effect on the anisotropy ratio of rates. Our calculations show that the inclusion of the internuclear motion increases the ratio. In particular, its value for H_2 is larger than that for D_2 by 2.2% at $F = 0.05$ and 1.5% at $F = 0.09$. This difference is consistent with the experimental results, as far as this can be judged from a single experimental point available for D_2. Why does the internuclear motion increase the ratio? To answer this question, let us estimate the difference between the anisotropy ratios for H_2 and D_2. We do this within ME-WFAT(0) in the limit $M \to \infty$, similar to how the isotope effect on the total ionization rate was treated in Ref. [27]. We approximate the solution to Eq. (22) by the ground state of a harmonic oscillator centered at $R = R_0$ and expand the exponent in the field factor (9) and the structure factor in Eq. (6) near $R = R_0$ up to the first-order terms. The result is

$$\frac{A(\mathrm{H}_2)}{A(\mathrm{D}_2)} = 1 - (c_\parallel - c_\perp)\frac{4\varkappa_{1s\sigma}(R_0)I'_{1s\sigma}}{\sqrt{2m_p V''_{\rm mol}}F}\left(1 - \frac{1}{\sqrt{2}}\right), \quad (26)$$

where $A = \Gamma_\parallel/\Gamma_\perp$ is the anisotropy ratio of rates shown in Fig. 10. Here $c_\parallel = c(\beta = 0^\circ)$ and $c_\perp = c(\beta = 90^\circ)$, where

$$c(\beta) = \frac{1}{G_{1s\sigma}(\mathbf{R})}\frac{dG_{1s\sigma}(\mathbf{R})}{dR}\bigg|_{R=R_0}, \quad (27)$$

$I'_{1s\sigma}$ is the first derivative of the ionization potential [see Eq. (10)],

$$I'_{1s\sigma} = \frac{dI_{1s\sigma}(R)}{dR}\bigg|_{R=R_0}, \quad (28)$$

and $V''_{\rm mol}$ is the second derivative of the molecular BO potential,

$$V''_{\rm mol} = \frac{d^2}{dR^2}\left[\frac{1}{R} + E_0^{(2)}(R)\right]_{R=R_0}. \quad (29)$$

The second term on the right-hand side of Eq. (26) gives the leading-order correction to the unity for $M \to \infty$. Equation (26) predicts that the anisotropy ratio for H_2 is larger than that for D_2 by 2.1% at $F = 0.05$ and 1.2% at $F = 0.09$, which is rather close to the difference between the ME-WFAT-P-S-N results. Thus, we can use Eq. (26) to understand the difference. We have $I'_{1s\sigma} < 0$, that is, the ionization potential decreases as R grows, which is expectable. We also have $c_\parallel > c_\perp$, because $G_{1s\sigma}(\mathbf{R}_\parallel)$ grows while $G_{1s\sigma}(\mathbf{R}_\perp)$ decreases with R (see Table I), and this is a less intuitive property. It is the latter property of the structure factor $G_{1s\sigma}(\mathbf{R})$ which makes the correction term on the right-hand side of Eq. (26) positive. This explains why the ratio on the left-hand side is larger than unity.

We close the discussion of the anisotropy ratio of ionization rates by a brief survey of previous theoretical calculations. The different calculations can be characterized by how they reproduce the three main features of the ratio: its absolute values, dependence on F, and the isotope effect. In a number of studies, the ratio was obtained as a field-independent constant calculated at $R = R_0$. This yielded a wide spectrum of values: 1.17 [31], 1.45 [32], 1.33 [17,18], and 1.37 [33], in calculations for a static field, and 1.4 [40] and 1.68 [41], in time-dependent calculations. This level of approximation corresponds to the present ME-WFAT(0); our result at this level 1.39 is consistent with Ref. [33]. Some studies predicted that the ratio, still calculated at $R = R_0$, depends on F. Thus, the ratio obtained in Ref. [29] decreases from 1.53 to 1.43 in the interval of F shown in Fig. 10, which correctly reproduces the slope of the dependence on F, but gives too large values. The ratio obtained in Ref. [36] decrease from 1.25 to 1.22 in the same interval, which lies slightly below the experimental results. In Ref. [38], the ratio calculated by two different time-dependent methods varies in the intervals

from 1.7 to 1.1 and from 2.2 to 1.8. At this level of approximation, the results should be compared with the present ME-WFAT-P-S. Our ME-WFAT-P-S results lie below the results of Ref. [36], and hence farther from the experimental results, but the slope of their dependence on F is closer to that in the experiment. We are not aware of previous calculations of the anisotropy ratio of rates with the internuclear motion included. Our best results including this effect, ME-WFAT-P-S-N, lie close to the experimental results. The level of their agreement with the experiment for H_2 is similar to that for the ratio of rates from Ref. [36]. In addition, the present theory describes the isotope effect not accounted for in Ref. [36].

We next discuss the anisotropy ratio of ionization yields. It generally differs from the ratio of rates because of depletion. The way how the effect of depletion should be taken into account depends on the experimental setup. Let us consider the case of circularly polarized pulses used in Refs. [29,30]. In these experiments, photoelectrons ejected from molecules aligned nearly parallel to the polarization plane were detected in coincidence with protons, which enabled one to determine the dependence of the ionization yield on the angle β between the molecular axis and the rotating electric field. For a given ionization rate $\Gamma(F,\beta)$ as a function of the ionizing field strength and the angle, the probability for the molecule to survive until time t is

$$P(t) = \exp\left[-\int_{-\infty}^{t} \Gamma(F(t'),\beta(t'))\,dt'\right], \tag{30}$$

where $\beta(t) = \omega t \pmod{\pi}$, with ω being the laser angular frequency, and $F(t)$ is the field strength in the pulse. The total ionization yield at a fixed β in the circular polarization (CP) case is given by the sum of the probabilities of ionization during small intervals of time Δt determined by the angular resolution of the photoelectron detector around moments $t_n = (\beta + n\pi)/\omega$, $n = 0, \pm 1, \ldots,$ at which $\beta(t_n) = \beta$, namely,

$$Y^{\rm CP}(F,\beta) = \Delta t \sum_n \Gamma(F(t_n),\beta) P(t_n), \tag{31}$$

where $F = \max[F(t)]$ is the pulse amplitude. Here we have neglected all field-induced processes but tunneling ionization. The experiments for H_2 [29] and D_2 [30] were performed with pulses of wavelengths 800 nm and 1850 nm, respectively. We model the field strength in these experiments by $F(t) = F\exp[-2\ln 2\,(t/\tau)^2]$, with the full width at half maximum of the pulse τ equal to 40 fs for H_2 [29] and 50 fs for D_2 [30] and the pulse amplitude F determined by the experimental intensity I from $I = cF^2/4\pi$. The survival probability (30) is evaluated using the ME-WFAT(0) ionization rate. The yields $Y_\parallel^{\rm CP}(F) = Y^{\rm CP}(F,\beta = 0^\circ)$ and $Y_\perp^{\rm CP}(F) = Y^{\rm CP}(F,\beta = 90^\circ)$ are calculated from Eq. (31) using the ME-WFAT-P-S-N rates given by Eqs. (23) and (24), respectively. Note that the interval Δt is common for both orientations, so it is canceled in the ratio. The ratios of the yields, $Y_\parallel^{\rm CP}(F)/Y_\perp^{\rm CP}(F)$, for H_2 and D_2 are shown by thick solid lines in Fig. 10. They turn out to be very close to the corresponding ratios of rates in the whole interval of F considered. This is explained as follows. For purely monochromatic pulses with the field strength $F(t) = F$ independent of t, the rate factor in (31) does not depend on n, and therefore the ratio of yields coincides with the ratio of rates. In this case, depletion does not reveal itself in the ratio, which is a remarkable property of experiments with circularly polarized pulses. For sufficiently long but finite pulses used in Refs. [29,30], the ratios of yields and rates do not coincide with each other, but the difference remains small even at stronger fields, where depletion becomes significant. Thus our conclusion concerning the importance of the different effects for the ratio of rates holds also for the ratio of yields.

It is worthwhile to mention that the dependence of the ionization yield on β can be also measured using linearly polarized pulses. Such an approach was demonstrated in a pump-probe experiment [56], where the pump and probe pulses were used to align and ionize molecules, respectively. Although the distribution of molecular alignment achieved in this particular experiment is rather broad, it can be made narrower. To demonstrate the difference from the circular polarization case we assume for simplicity that molecules are sharply aligned. Then, using the same notation as in Eq. (31), the total ionization yield at a fixed β in the linear polarization (LP) case is

$$Y^{\rm LP}(F,\beta) = 1 - \exp\left[-\int \Gamma(F(t),\beta)\,dt\right]. \tag{32}$$

This formula differs from Eq. (31). In particular, for monochromatic pulses with $F(t) = F\cos(\omega t)$ the ratio of yields (32) does not coincide with the ratio of rates, even if depletion is weak, because of the oscillating factor $\cos(\omega t)$, which makes the effective field strength smaller. We have calculated the yields $Y_\parallel^{\rm LP}(F) = Y^{\rm LP}(F,\beta = 0^\circ)$ and $Y_\perp^{\rm LP}(F) = Y^{\rm LP}(F,\beta = 90^\circ)$ and their ratio for H_2 and D_2 using Eq. (32). The results show that the effect of depletion on the anisotropy ratio in the linear polarization case is stronger than that in the circular polarization case. As F grows, the exponent in Eq. (32) vanishes for both orientations and the ratio of yields tends to unity. As a result, the ratio of yields at stronger fields behaves differently from the ratio of rates. We do not discuss these results in more detail here because they are not relevant to the comparison with the experiments [29,30].

The anisotropy ratios of ionization yields observed in Refs. [29,30] were modeled by time-dependent calculations in several studies. The calculations in Refs. [30,36] were performed for a fixed internuclear distance $R = R_0$, and hence do not account for the isotope effect. Besides, linearly polarized fields were considered in these calculations, meaning that the large depletion effect discussed above is embedded at stronger fields. In Ref. [30], the ratio calculated in the interval $0.05 < F < 0.085$ varies nonmonotonically in the interval 1.28-1.12 at 800 nm and decays from 1.2 to 1.12 at 1850 nm. These values are smaller than our results for circularly polarized pulses. In Ref. [36], Eq. (32) with time-independent rates was used and the resulting ratio monotonically decays from 1.27 to 1.14 at 800 nm and from 1.25 to 1.13 at 1850 nm. The rapid decrease of the ratios at stronger fields in these calculations was explained by depletion. In Refs. [34,37], time-dependent calculations with linearly polarized pulses including the internuclear motion were reported. In Ref. [34], the ratio of yields obtained at 400 nm varies nonmonotonically in the interval 0.5–1.8. These results do not belong to the adiabatic regime

and are rather far from the experiments [29,30]. However, they for the first time reproduced the isotope effect, that is, the fact that the ratio of yields for H_2 is larger than that for D_2. We conclude that, considering all three main features of the anisotropy ratio mentioned above (absolute values, dependence on F, and the isotope effect), the present theory including the correct treatment of depletion for circularly polarized pulses described by Eq. (31) demonstrates the best performance compared to the previous calculations.

V. CONCLUSION

We have presented a study of tunneling ionization of the hydrogen molecule. Our theory is based on the leading-order ME-WFAT [5] and successively incorporates the Stark-shift, core polarization, spectator nucleus, and internuclear motion effects. All the effects are shown to strongly affect the ionization rate. The predictions of the theory are in good agreement with the *ab initio* calculations for H_2 with frozen nuclei [14,15] and experiments on the anisotropy of ionization yields for H_2 [29] and D_2 [30]. The remaining difference between the present results and the *ab initio* calculations is attributed mainly to the field distortion of the initial state of H_2 and contribution to the core polarization effect from higher excited states of H_2^+ not included here. The difference between the theory and experimental results is in addition affected by nonadiabatic effects which violate the adiabatic approximation [2]. Our theory also predicts an isotope effect on the anisotropy ratio for H_2 and D_2, which is consistent with the experiments [29,30] and was not described by previous calculations. The effect is explained qualitatively in terms of properties of the structure factor for the dominant ionization channel.

ACKNOWLEDGMENT

This work was supported in part by JSPS KAKENHI Grant No. 19H00887.

[1] F. Krausz and M. Ivanov, Attosecond physics, Rev. Mod. Phys. **81**, 163 (2009).
[2] O. I. Tolstikhin and T. Morishita, Adiabatic theory of ionization by intense laser pulses: Finite-range potentials, Phys. Rev. A **86**, 043417 (2012).
[3] O. I. Tolstikhin, T. Morishita, and L. B. Madsen, Theory of tunneling ionization of molecules: Weak-field asymptotics including dipole effects, Phys. Rev. A **84**, 053423 (2011).
[4] V. H. Trinh, O. I. Tolstikhin, L. B. Madsen, and T. Morishita, First-order correction terms in the weak-field asymptotic theory of tunneling ionization, Phys. Rev. A **87**, 043426 (2013).
[5] O. I. Tolstikhin, L. B. Madsen, and T. Morishita, Weak-field asymptotic theory of tunneling ionization in many-electron atomic and molecular systems, Phys. Rev. A **89**, 013421 (2014).
[6] V. H. Trinh, O. I. Tolstikhin, and T. Morishita, Weak-field asymptotic theory of tunneling ionization: Benchmark analytical results for two-electron atoms, J. Phys. B **48**, 061003 (2015).
[7] V. H. Trinh, O. I. Tolstikhin, and T. Morishita, First-order correction terms in the weak-field asymptotic theory of tunneling ionization in many-electron systems, J. Phys. B **49**, 195603 (2016).
[8] V. H. Trinh, V. N. T. Pham, O. I. Tolstikhin, and T. Morishita, Weak-field asymptotic theory of tunneling ionization including the first-order correction terms: Application to molecules, Phys. Rev. A **91**, 063410 (2015).
[9] S. I. Themelis and C. A. Nicolaides, dc-field tunneling of polyelectronic atoms and of negative ions: Computations based on models and on *ab initio* theory, Phys. Rev. A **49**, 3089 (1994).
[10] A. Scrinzi, M. Geissler, and T. Brabec, Ionization Above the Coulomb Barrier, Phys. Rev. Lett. **83**, 706 (1999).
[11] S. I. Themelis, T. Mercouris, and C. A. Nicolaides, Quantum-mechanical versus semiclassical calculations of dc-field-induced tunneling rates for helium for field strengths in the range 0.067–1.0 a.u., Phys. Rev. A **61**, 024101 (1999).
[12] J. S. Parker, G. S. J. Armstrong, M. Boca, and K. T. Taylor, From the UV to the static-field limit: Rates and scaling laws of intense-field ionization of helium, J. Phys. B **42**, 134011 (2009).
[13] S. I. Themelis and C. A. Nicolaides, Complex energies and the polyelectronic Stark problem, J. Phys. B **33**, 5561 (2000).
[14] A. Saenz, Behavior of molecular hydrogen exposed to strong dc, ac, or low-frequency laser fields. II. Comparison of *ab initio* and Ammosov-Delone-Krainov rates, Phys. Rev. A **66**, 063408 (2002).
[15] T.-C. Jagau, Coupled-cluster treatment of molecular strong-field ionization, J. Chem. Phys. **148**, 204102 (2018).
[16] M. Hernández Vera and T.-C. Jagau, Resolution-of-the-identity second-order Møller-Plesset perturbation theory with complex basis functions: Benchmark calculations and applications to strong-field ionization of polyacenes, J. Chem. Phys. **152**, 174103 (2020).
[17] L. B. Madsen, O. I. Tolstikhin, and T. Morishita, Application of the weak-field asymptotic theory to the analysis of tunneling ionization of linear molecules, Phys. Rev. A **85**, 053404 (2012).
[18] R. Saito, O. I. Tolstikhin, L. B. Madsen, and T. Morishita, Structure factors for tunneling ionization rates of diatomic molecules, At. Data Nucl. Data Tables **103–104**, 4 (2015).
[19] L. B. Madsen, F. Jensen, O. I. Tolstikhin, and T. Morishita, Structure factors for tunneling ionization rates of molecules, Phys. Rev. A **87**, 013406 (2013).
[20] A. I. Dnestryan, O. I. Tolstikhin, L. B. Madsen, and F. Jensen, Structure factors for tunneling ionization rates of molecules: General grid-based methodology and convergence studies, J. Chem. Phys. **149**, 164107 (2018).
[21] A. I. Dnestryan, O. I. Tolstikhin, F. Jensen, and L. B. Madsen, Torsional effects in strong-field ionization of molecules, Phys. Rev. Research **1**, 023018 (2019).
[22] P. M. Kraus, B. Mignolet, D. Baykusheva, A. Rupenyan, L. Horný, E. F. Penka, G. Grassi, O. I. Tolstikhin, J. Schneider, F. Jensen *et al.*, Measurement and laser control of attosecond charge migration in ionized iodoacetylene, Science **350**, 790 (2015).
[23] T. Endo, A. Matsuda, M. Fushitani, T. Yasuike, O. I. Tolstikhin, T. Morishita, and A. Hishikawa, Imaging Electronic Excitation

of NO by Ultrafast Laser Tunneling Ionization, Phys. Rev. Lett. **116**, 163002 (2016).

[24] M. Okunishi, Y. Ito, V. Sharma, S. Aktar, K. Ueda, R. R. Lucchese, A. I. Dnestryan, O. I. Tolstikhin, S. Inoue, H. Matsui, and T. Morishita, Rescattering photoelectron spectroscopy of the CO_2 molecule: Progress towards experimental discrimination between theoretical target-structure models, Phys. Rev. A **100**, 053404 (2019).

[25] T. Endo, H. Fujise, H. Hasegawa, A. Matsuda, M. Fushitani, O. I. Tolstikhin, T. Morishita, and A. Hishikawa, Angle dependence of dissociative tunneling ionization of NO in asymmetric two-color intense laser fields, Phys. Rev. A **100**, 053422 (2019).

[26] P. K. Samygin, T. Morishita, and O. I. Tolstikhin, Weak-field asymptotic theory of tunneling ionization from nearly degenerate states, Phys. Rev. A **98**, 033401 (2018).

[27] O. I. Tolstikhin, H. J. Wörner, and T. Morishita, Effect of nuclear motion on tunneling ionization rates of molecules, Phys. Rev. A **87**, 041401(R) (2013).

[28] X. Wang, H. Xu, A. Atia-Tul-Noor, B. T. Hu, D. Kielpinski, R. T. Sang, and I. V. Litvinyuk, Isotope Effect in Tunneling Ionization of Neutral Hydrogen Molecules, Phys. Rev. Lett. **117**, 083003 (2016).

[29] A. Staudte, S. Patchkovskii, D. Pavičić, H. Akagi, O. Smirnova, D. Zeidler, M. Meckel, D. M. Villeneuve, R. Dörner, M. Y. Ivanov, and P. B. Corkum, Angular Tunneling Ionization Probability of Fixed-in-Space H_2 Molecules in Intense Laser Pulses, Phys. Rev. Lett. **102**, 033004 (2009).

[30] M. Magrakvelidze, F. He, S. De, I. Bocharova, D. Ray, U. Thumm, and I. V. Litvinyuk, Angular dependence of the strong-field ionization measured in randomly oriented hydrogen molecules, Phys. Rev. A **79**, 033408 (2009).

[31] X. M. Tong, Z. X. Zhao, and C. D. Lin, Theory of molecular tunneling ionization, Phys. Rev. A **66**, 033402 (2002).

[32] S.-F. Zhao, C. Jin, A.-T. Le, T. F. Jiang, and C. D. Lin, Determination of structure parameters in strong-field tunneling ionization theory of molecules, Phys. Rev. A **81**, 033423 (2010).

[33] L. Yue, S. Bauch, and L. B. Madsen, Electron correlation in tunneling ionization of diatomic molecules: An application of the many-electron weak-field asymptotic theory with a generalized-active-space partition scheme, Phys. Rev. A **96**, 043408 (2017).

[34] Y. V. Vanne and A. Saenz, Ionization of molecular hydrogen and deuterium by frequency-doubled Ti:sapphire laser pulses, Phys. Rev. A **80**, 053422 (2009).

[35] Y. V. Vanne and A. Saenz, Alignment-dependent ionization of molecular hydrogen in intense laser fields, Phys. Rev. A **82**, 011403(R) (2010).

[36] Y.-J. Jin, X.-M. Tong, and N. Toshima, Alignment-dependent ionization of hydrogen molecules in intense laser fields, Phys. Rev. A **83**, 063409 (2011).

[37] J. Förster, Y. V. Vanne, and A. Saenz, Ionization behavior of molecular hydrogen in intense laser fields: Influence of molecular vibration and alignment, Phys. Rev. A **90**, 053424 (2014).

[38] X. Chu, Time-dependent density-functional-theory calculation of strong-field ionization rates of H_2, Phys. Rev. A **82**, 023407 (2010).

[39] A. Russakoff and K. Varga, Time-dependent density-functional study of the ionization and fragmentation of C_2H_2 and H_2 by strong circularly polarized laser pulses, Phys. Rev. A **92**, 053413 (2015).

[40] W. Li and J. Liu, Two-center interference effects on the orientation dependence of the strong-field double-ionization yields for hydrogen molecules, Phys. Rev. A **86**, 033414 (2012).

[41] M.-M. Liu and Y. Liu, Semiclassical models for strong-field tunneling ionization of molecules, J. Phys. B **50**, 105602 (2017).

[42] A. Khan, D. Trabert, S. Eckart, M. Kunitski, T. Jahnke, and R. Dörner, Orientation-dependent dissociative ionization of H_2 in strong elliptic laser fields: Modification of the release time through molecular orientation, Phys. Rev. A **101**, 023409 (2020).

[43] H. Ibrahim, C. Lefebvre, A. D. Bandrauk, A. Staudte, and F. Légaré, H_2: The benchmark molecule for ultrafast science and technologies, J. Phys. B **51**, 042002 (2018).

[44] A. Saenz, On the influence of vibrational motion on strong-field ionization rates in molecules, J. Phys. B **33**, 4365 (2000).

[45] O. I. Tolstikhin and T. Morishita, Weak-field versus Born-Oppenheimer asymptotics in the theory of tunneling ionization of molecules, Phys. Rev. A **95**, 033410 (2017).

[46] K. Pachucki, M. Zientkiewicz, and V. A. Yerokhin, H2SOLV: Fortran solver for diatomic molecules in explicitly correlated exponential basis, Comput. Phys. Commun. **208**, 162 (2016).

[47] K. Pachucki, Born-Oppenheimer potential for H_2, Phys. Rev. A **82**, 032509 (2010).

[48] O. I. Tolstikhin and C. Namba, *CTBC—A Program to Solve the Colinear Three-Body Coulomb Problem: Bound States and Scattering below the Three-Body Disintegration Threshold* (National Institute for Fusion Science, Toki, Japan, 2003).

[49] A. I. Dnestryan and O. I. Tolstikhin, Integral-equation approach to the weak-field asymptotic theory of tunneling ionization, Phys. Rev. A **93**, 033412 (2016).

[50] J. Rychlewski, An accurate calculation of the polarizability of the hydrogen molecule and its dependence on rotation, vibration and isotopic substitution, Mol. Phys. **41**, 833 (1980).

[51] A. Saenz, Enhanced ionization of molecular hydrogen in very strong fields, Phys. Rev. A **61**, 051402(R) (2000).

[52] A. Saenz, Behavior of molecular hydrogen exposed to strong dc, ac, or low-frequency laser fields. I. Bond softening and enhanced ionization, Phys. Rev. A **66**, 063407 (2002).

[53] D. Pavičić, K. F. Lee, D. M. Rayner, P. B. Corkum, and D. M. Villeneuve, Direct Measurement of the Angular Dependence of Ionization for N_2, O_2, and CO_2 in Intense Laser Fields, Phys. Rev. Lett. **98**, 243001 (2007).

[54] H. Akagi, T. Otobe, A. Staudte, A. Shiner, F. Turner, R. Dörner, D. M. Villeneuve, and P. B. Corkum, Laser tunnel ionization from multiple orbitals in HCl, Science **325**, 1364 (2009).

[55] J. Wu, L. P. H. Schmidt, M. Kunitski, M. Meckel, S. Voss, H. Sann, H. Kim, T. Jahnke, A. Czasch, and R. Dörner, Multiorbital Tunneling Ionization of the CO Molecule, Phys. Rev. Lett. **108**, 183001 (2012).

[56] X. Xie, K. Doblhoff-Dier, H. Xu, S. Roither, M. S. Schöffler, D. Kartashov, S. Erattupuzha, T. Rathje, G. G. Paulus, K. Yamanouchi *et al.*, Selective Control Over Fragmentation Reactions in Polyatomic Molecules Using Impulsive Laser Alignment, Phys. Rev. Lett. **112**, 163003 (2014).